



Contents lists available at ScienceDirect

## Bioorganic &amp; Medicinal Chemistry Letters

journal homepage: [www.elsevier.com/locate/bmcl](http://www.elsevier.com/locate/bmcl)

## Ligand-based virtual screen for the discovery of novel M<sub>5</sub> inhibitor chemotypes



Alexander R. Geanes<sup>c,†</sup>, Hykeyung P. Cho<sup>a,b,†</sup>, Kellie D. Nance<sup>a,c</sup>, Kevin M. McGowan<sup>a,b</sup>, P. Jeffrey Conn<sup>a,b,d</sup>, Carrie K. Jones<sup>a,b,d</sup>, Jens Meiler<sup>c,\*</sup>, Craig W. Lindsley<sup>a,b,c,d,\*</sup>

<sup>a</sup> Vanderbilt Center for Neuroscience Drug Discovery, Vanderbilt University School of Medicine, Nashville, TN 37232, USA

<sup>b</sup> Department of Pharmacology, Vanderbilt University School of Medicine, Nashville, TN 37232, USA

<sup>c</sup> Department of Chemistry, Vanderbilt University, Nashville, TN 37232, USA

<sup>d</sup> Vanderbilt Center for Addiction Research, Vanderbilt University School of Medicine, Nashville, TN 37232, USA

## ARTICLE INFO

## Article history:

Received 20 July 2016

Revised 27 July 2016

Accepted 28 July 2016

Available online 30 July 2016

## Keywords:

M<sub>5</sub>

Muscarinic acetylcholine receptor

Virtual screen

Structure–activity relationship (SAR)

## ABSTRACT

This Letter describes a ligand-based virtual screening campaign utilizing SAR data around the M<sub>5</sub> NAMs, ML375 and VU6000181. Both QSAR and shape scores were employed to virtually screen a 98,000-member compound library. Neither approach alone proved productive, but a consensus score of the two models identified a novel scaffold which proved to be a modestly selective, but weak inhibitor (VU0549108) of the M<sub>5</sub> mAChR (M<sub>5</sub> IC<sub>50</sub> = 6.2 μM, M<sub>1–4</sub> IC<sub>50</sub>s > 10 μM) based on an unusual 8-((1,3,5-trimethyl-1H-pyrazol-4-yl)sulfonyl)-1-oxa-4-thia-8-azaspiro[4,5]decane scaffold. [<sup>3</sup>H]-NMS binding studies showed that VU0549108 interacts with the orthosteric site (K<sub>i</sub> of 2.7 μM), but it is not clear if this is negative cooperativity or orthosteric binding. Interestingly, analogs synthesized around VU0549108 proved weak, and SAR was very steep. However, this campaign validated the approach and warranted further expansion to identify additional novel chemotypes.

© 2016 Elsevier Ltd. All rights reserved.

Recently, we reported on the results of a functional high-throughput screen to identify highly selective muscarinic acetylcholine receptor subtype 5 (M<sub>5</sub>) inhibitors (both negative allosteric modulators (NAMs)<sup>1,2</sup> and orthosteric antagonists<sup>3</sup>). Based on the strong genetic data linking this receptor to addiction,<sup>4–6</sup> pharmacological recapitulation with a small molecule is of great interest. Subsequent optimization did lead to the discovery the first highly selective and CNS penetrant M<sub>5</sub> NAMs, ML375 (**1**) and VU6000181 (**2**); however, SAR was steep. Moreover, we were attracted to the rigid concave/convex topology of the core of **1** and **2** (see X-ray crystal structure **3**, see Fig. 1<sup>1</sup>), and, based on prior machine learning/virtual screening success with mGlu<sub>5</sub> NAMs,<sup>7</sup> felt this scaffold was a viable lead for a ligand-based virtual screening exercise to identify new M<sub>5</sub> chemotypes. In this Letter, we will describe the methodology employed for the discovery of a novel M<sub>5</sub> inhibitor chemotype.

The medicinal chemistry effort surrounding the ML375 scaffold resulted in 68 active compounds with varying levels of potency and 145 inactive compounds (M<sub>5</sub> IC<sub>50</sub>s > 10 μM). This information

made it possible to build artificial neural network (ANN) quantitative structure–activity relationship (QSAR) models to correlate molecular features with biological activity.<sup>8</sup> In addition, the rigid structure of the ML375 scaffold (only 3 rotatable bonds) defines a limited conformational space and made shape-based similarity metrics an attractive option as well.<sup>9</sup>

Molecular descriptor calculation, ANN training, and model analyses were performed using the BioChemical Library (BCL) developed at Vanderbilt University.<sup>8</sup> The dataset was prepared by removing any ions from structures, adding hydrogens, neutralizing charges, and removing duplicate entries. A single three-dimensional conformation was generated for each structure using Corina version 3.60.<sup>10</sup> Descriptors which encoded 1D (scalar values), 2D (connectivity), and 3D (shape) information were calculated for each structure. Scalar descriptors included number of hydrogen bond donors and acceptors, calculated LogP, and topological polar surface area. 2- and 3-D information was encoded using autocorrelation functions weighted by properties such as partial charge and polarizability.<sup>11</sup> These descriptors resulted in 1315 numerical values for each structure. Calculated descriptor vectors were labeled with the respective human M<sub>5</sub> pIC<sub>50</sub> value, or 0 if the compound was inactive. A feed-forward neural network with a densely connected 32-node hidden layer and a single-valued output layer was trained using this feature set. For training, error values were

\* Corresponding authors.

E-mail addresses: [jens.meiler@vanderbilt.edu](mailto:jens.meiler@vanderbilt.edu) (J. Meiler), [craig.lindsley@vanderbilt.edu](mailto:craig.lindsley@vanderbilt.edu) (C.W. Lindsley).

† These authors contributed equally.

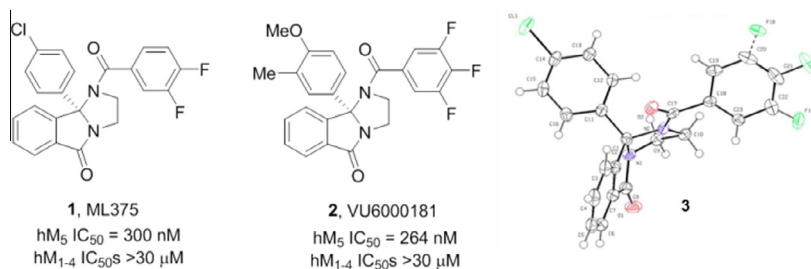


**Figure 1.** Structures of M<sub>5</sub> NAM ML375 (1), VU6000181 (2) and the X-ray crystal structure 3 of 1, highlighting the rigid structure of the core.

calculated by treating pIC<sub>50</sub> values as binary values based on whether pIC<sub>50</sub> was greater than 5 (active) or less than 5 (inactive). A 5-fold cross validation procedure using monitoring and independent sets and dropout was used to prevent overtraining and to evaluate model performance.<sup>11</sup> Receiver-operator characteristic (ROC) curves and figures of merit are shown in Figure 2A and indicate that the models were able to classify active compounds over inactives at a rate substantially higher than random chance.

In addition, 1 and 2 were selected for the generation of a 3-dimensional binding hypothesis. These two compounds were aligned using the flexible alignment feature of Surflex-Sim from Sybyl 2.1.1.<sup>9</sup> Default parameter values for the algorithm were used with the exception that ring flexibility was considered during the alignment. The highest-scoring hypothesis from the alignment was used for virtual screening (Fig. 2B). A receiver-operator characteristic (ROC) curve for this hypothesis generated by aligning and scoring the remaining 211 compounds from the M<sub>5</sub> NAM dataset with the flexible screening (pscreen) feature of Surflex-Sim is shown in Figure 2A. The shape based model was also able to prioritize active compounds over inactives at a rate higher than random chance. The shape-based model resulted in similar predictive ability to the QSAR model for high-scoring compounds, though the QSAR models appeared to outperform the shape model across the whole dataset.

Each model was used to independently select 30 compounds from an in-house 98,000-compound screening library for experimental testing. The character of the top compounds from each model differed substantially from each other, though there were many substructural commonalities in the compounds of both sets. The QSAR model preferentially chose compounds from the same scaffold pool, whereas the shape-based method contained more diverse chemical structures. From this set of 60 compounds, two compounds from the shape-based set, VU0101217 and VU0627194, showed weak antagonist activity at M<sub>5</sub>, exhibiting around 40 percent inhibition of M<sub>5</sub> response at 30 μM (Fig. 3). This indicated that a diverse selection could be more powerful for compound discovery than an exhaustive enumeration of SAR around a high scoring scaffold.

To leverage the predictive ability of both models, a larger screen using a consensus approach was performed. To address the issue of low compound diversity when prioritizing by QSAR score alone, the workflow involved first scoring the full 98,000-compound database with the ANN-QSAR models and clustering the highest-scoring 10 percent of the data to select a diverse set of high-scoring chemical structures. To enable clustering, a random subset was sampled from the prioritized compounds, Murcko scaffolds<sup>12</sup> were generated for each selected compound, and the maximum common substructure between each pair of Murcko scaffolds was calculated. Ring and chain fragments from each scaffold were also added to supplement the database. Fingerprint vectors were computed by searching for the presence of each substructure in the prioritized compounds. The distance metric between pairs of compounds was calculated as the Tanimoto<sup>13</sup> coefficient between fingerprint vectors.

A consensus score was calculated by scoring the top two highest QSAR-scoring compounds from each cluster (or a single compound if the cluster size was 1) with the shape-based method and combining the individual model scores. 986 compounds were aligned to the ML375 binding hypothesis in this manner using the Surflex-Sim 'pscreen' algorithm. The QSAR and Surflex scores were normalized such that their ranges fell between 0 and 1, and both normalized scores were added together to provide the final consensus score for each molecule. The 320 highest scoring compounds according to consensus score were selected and submitted for pharmacological screening against mAChR M<sub>5</sub>.

Using the two-model consensus approach, two compounds VU0549108 and VU0624456 demonstrated significant M<sub>5</sub> antagonist activity (maximum M<sub>5</sub> inhibition of 50 and 70 percent, respectively in a single point M<sub>5</sub> inhibition assay at 10 μM), and were confirmed with 10-point concentration response curves (M<sub>5</sub> IC<sub>50</sub>S of 3.86 μM and 5.16 μM, respectively employing the HTS DMSO stock). By QSAR score, VU0549108 was rank 1284 and VU0624456 was rank 3073 (with rank 1 being the best score). By shape score VU0549108 was rank 3520 and VU0624456 was rank 2446. In order to rapidly explore SAR surrounding the initially more attractive VU0624456 scaffold, SAR-by-catalog was performed by ordering a set of analogs from commercial sources. In addition, compounds that had a high similarity to the two hit compounds (2D fingerprint similarity with Tanimoto >0.5), and a second set of virtually screened compounds using updated models were chosen from the in-house screening library to follow up these results (Table 1). Single point screening revealed several possible antagonists which were subsequently confirmed using 10-point CRCs against M<sub>5</sub>. However, only analogs of the original hits showed significant M<sub>5</sub> activity, and none proved more potent than the original compounds.

These data prompted the resynthesis of VU0549108 (4) to reconfirm mAChR activity from fresh powder, as the lack of mAChR selectivity deprioritized VU0624456.<sup>14</sup> VU0549108 (4) was readily prepared in two steps (Scheme 1). Starting from commercial piperidine hydrate 5, treatment with sulfonyl chloride 6 provides 7 in 76% yield. Condensation with 2-mercaptoethanol under Lewis acid catalysis affords 4 in 79% yield. This expedited route was also employed for analog synthesis.

The resynthesized 4 proved to be a functional inhibitor of M<sub>5</sub> (Fig. 4A), with greater activity in the 10 μM single point assay (88%), an IC<sub>50</sub> of 6.2 μM (pIC<sub>50</sub> = 6.18 ± 0.09, ACh min 12.6 ± 2.5), and modest selectivity versus M<sub>1-4</sub> (IC<sub>50</sub>S >10 μM). The divergence from classical orthosteric antagonist chemotype, coupled with the observed selectivity, led us to perform radioligand binding assays to assess if 4 was an allosteric ligand (NAM) or an atypical orthosteric ligand. Here, employing the standard [<sup>3</sup>H]-NMS ligand (Fig. 4B),<sup>1-3</sup> and compared to atropine, 4 proved to interact with or modulate with orthosteric site with a K<sub>i</sub> of 2.7 μM (atropine control, K<sub>i</sub> = 2.7 nM).<sup>1-3,15-17</sup>

However, the effect on NMS binding could be due to cooperativity with the orthosteric site by binding of 4 to an allosteric site, or it

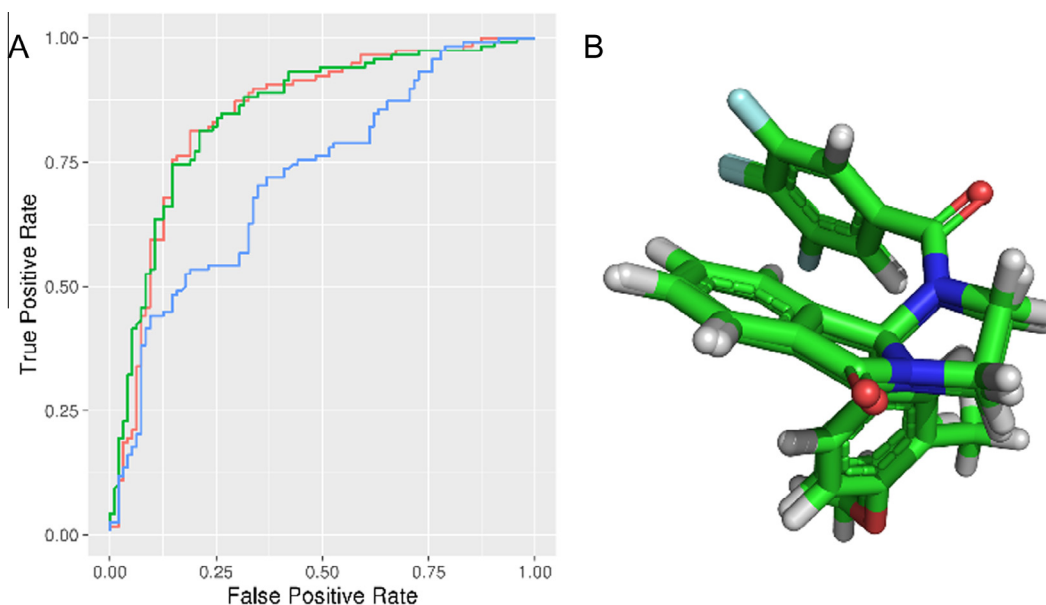


**Figure 2.** QSAR and shape-based models. (A) Receiver operator characteristic curves for Surflex-Sim shape (blue), QSAR (green), and QSAR + shape consensus (red) models. Area under the curve, QSAR: 0.85, Surflex: 0.72, Consensus: 0.84, random: 0.5. Average enrichment at 10% FPR, QSAR: 1.64, Surflex: 1.48, Consensus: 1.44, random: 1.0. (B) Highest-scoring Surflex-Sim hypothesis of VU6000181 and ML375. This hypothesis was used for the shape-based portion of the virtual screening workflow.

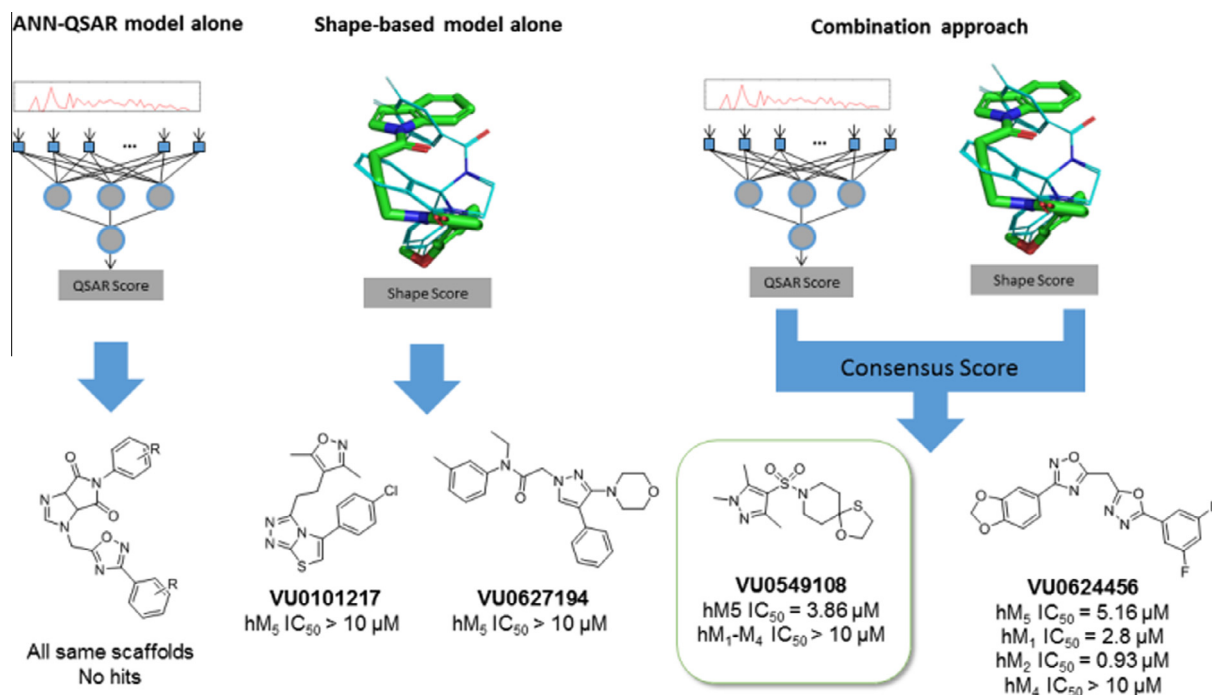
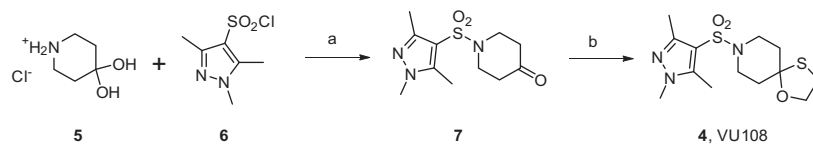


**Figure 3.** Summary of hit compounds discovered by the three distinct approaches. The consensus approach yielded the best result of the three with VU0549108 demonstrating selectivity for the  $M_5$  receptor over other mAChR isoforms, based on assay data employing HTS DMSO stock.

**Table 1**  
Sources and counts of compounds used to explore SAR around VU0549108 and VU0624456

Selection approach	Source	Number of compounds
2D similarity, VU0549108	In-house library	46
2D similarity, VU0624456	In-house library	37
VU0624456 analogs	Commercial	67
Virtual screening (consensus)	In-house library	237

could reflect direct, competitive interaction at the orthosteric site. Based on **4** being a small, non-basic chemotype, distinct from prototypical mAChR antagonists, and some measure of mAChR selectivity, more potent analogs are required to definitively address the mode of inhibition of  $M_5$ . Moreover, shape-based alignment of **1** and **4** (Fig. 5), while showing reasonable overlap for achiral **4**, significant lipophilic regions are not occupied. This hypothesis shows an alignment of one sulfonyl oxygen and the free pyrazole nitrogen in **4** align with the carbonyl groups in **1**, and the 4-oxathiolane oriented along the 9b-4-chlorophenyl group of **1**. Since the 4-



**Scheme 1.** Synthesis of VU0549108 (**4**). Reagents and conditions: (a) Triethylamine, DCM, rt 12 h, 76%; (b) 2-mercaptoethanol,  $\text{BF}_3 \cdot \text{OEt}_2$ , DCM, 12 h rt, 79%.

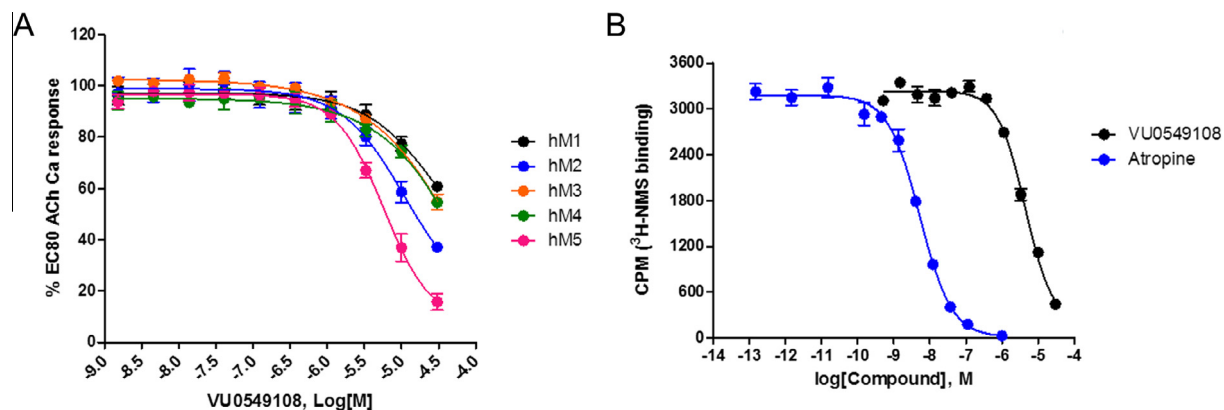


**Figure 4.** Molecular pharmacology profile of VU0549108 (**4**). (A) Concentration–response curves of **4** for human  $\text{hM}_5$ , as well as  $\text{hM}_{1-4}$  ( $\text{IC}_{50} > 10 \mu\text{M}$ ),  $n = 3$ . At  $30 \mu\text{M}$ , % Ach Min (Ave  $\pm$  SEM):  $\text{hM}_1$ ,  $61 \pm 2\%$ ;  $\text{hM}_2$ ,  $37 \pm 2\%$ ;  $\text{hM}_3$ ,  $55 \pm 3\%$ ;  $\text{hM}_4$ ,  $55 \pm 1\%$ ;  $\text{hM}_5$ ,  $16 \pm 2\%$ . B  $[^3\text{H}]\text{-N}$ -methylscopolamine (NMS) competition binding ( $n = 3$ ) in membranes prepared from human  $\text{M}_5$ -expressing cells, showing interaction (either allosteric cooperativity or orthosteric displacement;  $K_1 = 2.7 \mu\text{M}$ ).

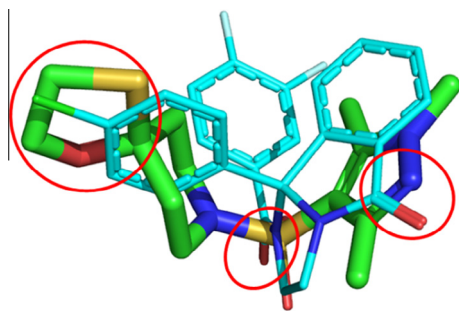


**Figure 5.** Overlay of **4** (green) on **1** (cyan). Hydrogen bond acceptors at the pyrazole and sulfonyl groups of **4** align with corresponding hydrogen bond acceptors in **1**, and the oxathiolane of **4** overlaps with the 4-chlorophenyl moiety of **1**. The overlap of these features could explain why the virtual screen selected **4**.

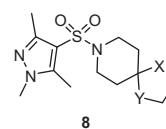
chlorophenyl group confers stereochemistry to ML375, this three-point pharmacophore could hold the structure in a position that allows **4** to mimic the stereochemistry of **1** without itself being chiral, and suggests why the virtual screen identified **4**.

A small library was synthesized to further explore SAR surrounding the **4** scaffold in hopes of increasing  $\text{M}_5$  inhibitory potency. Two points were considered for modification, namely the oxathiolane spirocycle, analogs **8** (Table 2) and the heterocyclic sulfonamide congeners, **9** (Table 3). SAR was steep,<sup>15–17</sup> with all analogs displaying  $\text{IC}_{50}\text{s} > 10 \mu\text{M}$ ; however, the  $\text{EC}_{80}$  was diminished. The 1,3-oxathiolane (**4**) was critical for activity, as the parent piperidinone, 1,3-dithiolane (**8a**), 1,3-dioxolane (**8b**) and spiro furan (**8c**) analogs all showed weak inhibition of  $\text{M}_5$  ( $\text{IC}_{50}\text{s} > 10 \mu\text{M}$ , single point % inhibition at  $10 \mu\text{M}$  from 37–86%). Similarly, only the 1,3,5-pyrazole sulfonamide of **4** maintained  $\text{M}_5$  inhibition.

In summary, a virtual screening campaign was conducted which employed a combination of an ANN-QSAR modeling approach with a shape-based modeling approach based on a rigid  $\text{M}_5$  NAM chemotype. This exercise identified a novel  $\text{M}_5$  ligand VU0549108 (**4**) derived from an unusual 8-((1,3,5-trimethyl-1H-

**Table 2**

Structure and activities of analogs **8**<sup>a</sup>

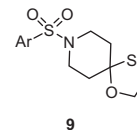


Compound	X	Y	$\text{hM}_5$ percent inhibition
<b>4</b> (VU0549108)	S	O	84% ( $\text{hM}_5 \text{ IC}_{50} = 6.18 \mu\text{M}$ )
<b>8a</b>	S	S	86%
<b>8b</b>	O	O	45%
<b>8c</b>	O	$\text{CH}_2$	37%

<sup>a</sup> Average of three determinations with  $\text{hM}_5$  cells with an  $\text{EC}_{80}$  of Ach as a single point % inhibition at  $10 \mu\text{M}$ . If not  $\text{IC}_{50}$  reported, the  $\text{IC}_{50}$  was  $> 10 \mu\text{M}$ .

**Table 3**

Structure and activities of analogs **9**<sup>a</sup>



Compound	Ar	$\text{hM}_5$ percent inhibition
<b>4</b> (VU0549108)	1,3,5-TriMe-1H-4-pyrazole	84% ( $\text{hM}_5 \text{ IC}_{50} = 6.18 \mu\text{M}$ )
<b>9a</b>	1-Me-1H-4-pyrazole	27%
<b>9b</b>	1,3-DiMe-1H-4-pyrazole	Inactive
<b>9c</b>	1,5-DiMe-1H-4-pyrazole	83%
<b>9d</b>	3-Cl-4-F-phenyl	83%
<b>9e</b>	3,5-DiF-phenyl	62%
<b>9f</b>	3,4,5-TriF-phenyl	55%
<b>9g</b>	3,5-DiMe-4-isoxazole	40%
<b>9h</b>	1-Me-4-imidazole	Inactive

<sup>a</sup> Average of three determinations with  $\text{hM}_5$  cells with an  $\text{EC}_{80}$  of Ach as a single point % inhibition at  $10 \mu\text{M}$ . If not  $\text{IC}_{50}$  reported, the  $\text{IC}_{50}$  was  $> 10 \mu\text{M}$ .

pyrazol-4-yl)sulfonyl)-1-oxa-4-thia-8-azaspiro[4,5]decane scaffold, characterized by steep SAR, modest selectivity versus M<sub>1-4</sub> and an a noted interaction with the orthosteric site in [<sup>3</sup>H]-NMS binding studies (studies to determine if allosteric cooperativity or orthosteric binding are in progress). Interestingly, neither model alone produced a hit from the virtual screen, but the combination of the two proved successful to identify a new M<sub>5</sub> inhibitor chemotype. These initial data argue well for validation of these approaches and warrant further expansion to identify additional novel M<sub>5</sub> chemotypes. Further work is in progress and will be reported in due course.

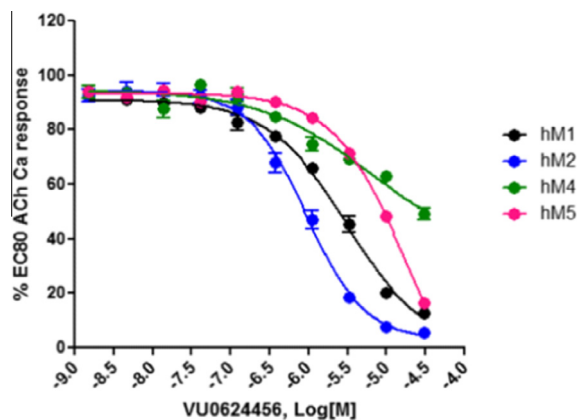
### Acknowledgments

We thank the NIH for funding via the National Institute of Drug Abuse (1R01DA037207) and the Chemistry-Biology Interface Research Training Program. Work in the Meiler laboratory is supported through NIH (R01 GM080403, R01 GM099842, R01 DK097376) and NSF (CHE 1305874). We also thank William K. Warren, Jr. and the William K. Warren Foundation who funded the William K. Warren, Jr. Chair in Medicine (to C.W.L.).

### References and notes

- Gentry, P. R.; Kokubo, M.; Bridges, T. M.; Byun, N.; Cho, H. P.; Smith, E.; Hodder, P. S.; Niswender, C. M.; Daniels, J. S.; Conn, P. J.; Lindsley, C. W.; Wood, M. R. *J. Med. Chem.* **2014**, *57*, 7804.
- Kurata, H.; Gentry, P. R.; Kokubo, M.; Cho, H. P.; Bridges, T. M.; Niswender, C. M.; Byers, F. W.; Wood, M. R.; Daniels, J. S.; Conn, P. J.; Lindsley, C. W. *Bioorg. Med. Chem. Lett.* **2015**, *25*, 690.
- Gentry, P. R.; Kokubo, M.; Bridges, T. M.; Cho, H. P.; Smith, E.; Chase, P.; Hodder, P. S.; Utley, T. J.; Rajapakse, A.; Byers, F.; Niswender, C. M.; Morrison, R. D.; Daniels, J. S.; Wood, M. R.; Conn, P. J.; Lindsley, C. W. *ChemMedChem* **2014**, *9*, 1677.
- Basile, A. S.; Fedorova, I.; Zapata, A.; Liu, X.; Shippenberg, T.; Duttaroy, A.; Yamada, M.; Wess, J. *Proc. Natl. Acad. Sci. U.S.A.* **2002**, *99*, 11452.

- Fink-Jensen, A.; Fedorova, I.; Wörtwein, G.; Woldbye, D. P.; Rasmussen, T.; Thomsen, M.; Bolwig, T. G.; Knitowski, K. M.; McKinzie, D. L.; Yamada, M.; Wess, J.; Basile, A. *J. Neurosci. Res.* **2003**, *74*, 91.
- Thomsen, M.; Woldbye, D. P.; Wortwein, G.; Fink-Jensen, A.; Wess, J.; Caine, S. B. *J. Neurosci.* **2005**, *25*, 8141.
- Mueller, R.; Dawson, E. S.; Meiler, J.; Chauder, B. A.; Bates, B. S.; Felts, A. S.; Lamb, J. P.; Menon, U. N.; Jadhav, S. B.; Kane, A. S.; Jones, C. K.; Rodriguez, A. L.; Conn, P. J.; Olsen, C. M.; Winder, D. G.; Emmitte, K. A.; Lindsley, C. W. *ChemMedChem* **2012**, *7*, 406.
- Butkiewicz, M.; Lowe, E. W., Jr.; Mueller, R.; Mendenhall, J. L.; Teixeira, P. L.; Weaver, C. D.; Meiler, J. *Molecules* **2013**, *18*, 735.
- Jain, A. N. *J. Med. Chem.* **2004**, *47*, 947.
- Sadowski, J. J. *Comput. Aided Mol. Des.* **1997**, *11*, 53.
- Mendenhall, J.; Meiler, J. *Comput. Aided Mol. Des.* **2016**, *30*, 177.
- Bemis, G. W.; Murcko, M. A. *J. Med. Chem.* **1996**, *39*, 2887.
- Willett, P. J. *Chem. Inf. Comput. Sci.* **1998**, *38*, 983.
- Concentration response curves for VU0624456 against hM<sub>1-5</sub>:



- Melancon, B. J.; Hopkins, C. R.; Wood, M. R.; Emmitte, K. A.; Niswender, C. M.; Christopoulos, A.; Conn, P. J.; Lindsley, C. W. *J. Med. Chem.* **2012**, *55*, 1445.
- Conn, P. J.; Lindsley, C. W.; Meiler, J.; Niswender, C. M. *Nat. Rev. Drug Disc.* **2014**, *13*, 692.
- Lindsley, C. W.; Emmitte, K. A.; Hopkins, C. R.; Bridges, T. M.; Gregory, K. A.; Niswender, C. M.; Conn, P. J. *Chem. Rev.* **2016**, *116*, 6707.